Spectrochimica Acta Part A 79 (2011) 6–16

Contents lists available at ScienceDirect

Spectrochimica Acta Part A: Molecular and Biomolecular Spectroscopy

journal homepage: www.elsevier.com/locate/saa

A physiochemical study of excited state intramolecular proton transfer process Luminescent chemosensor by spectroscopic investigation supported by *ab initio* calculations

Jayaraman Jayabharathi*, Venugopal Thanikachalam, Karunamoorthy Jayamoorthy, Marimuthu Venkatesh Perumal

Department of Chemistry, Annamalai University, Annamalainagar 608 002, India

ARTICLE INFO

Article history:
Received 6 October 2010
Received in revised form 8 November 2010
Accepted 9 December 2010

Keywords:
Nuclear magnetic resonance (NMR)
Ab initio calculations
Photoluminescence spectroscopy
Electrical properties

ABSTRACT

A group of novel Schiff base derivatives were synthesized and characterized by NMR spectra, X-ray, mass and CHN analysis. An excited state intramolecular proton transfer (ESIPT) process in hydroxy Schiff base (SB**4**) has been studied using emission spectroscopy and it was detected that the two distinct ground state isomers of I and II are responsible for the emission. The comparison of the emission wavelength in hydrocarbon solvent strongly supports that *trans* enol form predominates over the *cis* enol form for Schiff base (SB**4**). With increasing base concentration of the solutions of hydroxy substituted Schiff bases (SB**4** and SB**5**), two isobestic points are found which confirm the equilibrium among the *trans* enol form, anion and the *cis* enol form. The fluorescence of (SB**4**) quenched markedly with the gradual addition of Cu^{2+} but the fluorescence properties of (SB**5**) was influenced by other metal ions. Therefore Schiff base (SB**5**) can be used as a new fluorescence sensor to detect the quantity of Cu^{2+} ion in any sample solution depending on the relative intensity change. DFT calculations on energy, dipole moment, charge distribution of the rotamers in the ground and excited states of the Schiff base derivatives were performed and discussed. PES calculation indicates that the energy barrier for the interconversion of two rotamers is too high in the excited state than the ground state.

1. Introduction

Azo compounds are versatile molecules and have received much attention in research in the view of both fundamental and applications [1]. Apart from their purely chemical interest, azomethine dyes are being increasingly used in the textile, leather and plastic industries. Regarding the industrial importance of metallized azo dyes relative to their structures, they can be classified into two main types, i.e., those in which the azo group participates in coordination to the metal ion with formation of the chelate ring and those in which it is not [2]. Schiff bases derived from the salicylaldehydes are known as polydentate ligands, coordinating in deprotonated or neutral forms [1]. Schiff base ligands are potentially capable of forming stable complexes with metal ions [3] and shows excellent catalytic activity [4,5]. Various analytical methods including atomic emission or mass spectroscopy (ICP-AES and ICP-MS) have been widely used for the detection of heavy metals even at very low concentrations. However, these methods are relatively expensive and difficult to be applied. To solve this problem, a series of fluorescence sensors have been developed so far [6–10]. So, development of new fluorescent agents containing chelating groups can help to detect heavy metals more efficiently.

Copper is one of the important trace elements existing in human body, plants and animals. However, high amount of this element can cause serious health problems such as nausea, vomiting and diarrhea as well as damage to liver and kidneys [11]. Therefore, in the view of the biological and environmental importances, considerable attention has been focused on detection of Cu(II) ion [12,13]. The studies developed in this area usually depend on quenching of fluorescence intensity of the employed sensing material [14–17].

In addition, metal chelates play an essential role in the chemistry of living organisms and a large number of metal proteins and other metal complexes of biological importance have been studied [18,19]. Because of the importance of azo-containing Schiff base compounds and in continuance of the interest in the syntheses of azo-based compounds, herein syntheses and characterization of a series of azo-linked Schiff bases (**1**–**6**) namely, (0E,4E)-4-(2-phenyldiazenyl)-N-benzylidenebenzenamine (SB**1**), (0E,4E)-4-(2-phenyldiazenyl)-N-(*p*-N,N-dimethylaminobenzylidene)benzenamine (SB**2**), (0E,4E)-4-(2-phenyldiazenyl)-N-(*o*-

* Corresponding author. Tel.: +91 4144 239523.
E-mail address: jtchalam2005@yahoo.co.in (J. Jayabharathi).

1386-1425/$ – see front matter © 2010 Elsevier B.V. All rights reserved.
doi:10.1016/j.saa.2010.12.027

methoxy-benzylidene)benzenamine(SB**3**), (0E,4E)-4-(2-phenyldiazenyl)-N-(*m*-hydroxybenzylidene)benzenamine(SB**4**), (0E,4E)-4-(2-phenyldiazenyl)-N-(*o*-hydroxy-*m*-bromobenzylidene)benzenamine (SB**5**) and (0E,4E)-4-(2-phenyldiazenyl)-N-(*p*-hydroxy-*m*-methoxybenzylidene)benzenamine (SB**6**) are reported, their structures were confirmed by elemental, mass, IR and NMR analyses. Photophysical and photochemical studies of Schiff bases (**1**–**6**) were carried out and discussed in detail. The Schiff base (SB**5**) was developed as a possible Cu(II)-selective fluorescence sensor. Theoretical calculations were carried out using Gaussian-03 program [20,21] to supplement the experimental results.

2. Experimental

2.1. Materials and methods

Aniline (Sigma–Aldrich Ltd.), *p*-methoxybenzaldehyde, *p*-bromo-*o*-hydroxybenzaldehyde, N,N-dimethylaminobenzaldehyde, vanillin and *m*-hydroxybenzaldehyde (S.D. fine) and all other reagents were used without further purification.

2.2. Optical measurements and composition analysis

NMR spectra were recorded for Schiff bases (**1**–**6**) on a Bruker 400 MHz. The ultraviolet–visible (UV–Vis) spectra were measured on a UV–Vis spectrophotometer (Perkin Elmer, Lambda 35) and corrected for background due to solvent absorption. Photoluminescence (PL) spectra were recorded on a (Perkin Elmer LS55) fluorescence spectrometer. MS spectra were recorded on a Varian Saturn 2200 GCMS spectrometer.

2.3. Non-linear optical measurements

Its second harmonic generation efficiency was assessed by Kurtz powder technique [22] at IISc., Bangalore, India. It is a well established tool to evaluate the conversion efficiency of nonlinear optical materials. A Q-switched Nd:YAG laser operating at the fundamental wavelength of 1064 nm, generating about 4.1 mJ and pulse width of 8 ns was used for the present experimental study. The input laser beam was passed through an IR reflector and then incident on the powder form of the Schiff bases (**1**–**6**), which was packed in a glass capillary tube. The output energy was detected by a photodiode detector integrated with oscilloscope assembly.

2.4. Cyclic voltametry

Cyclic voltammetry (CV) analysis was performed using CHI 604C electrochemical analyzer, working electrode is glassy carbon electrode (GCE) diameter: 1 mm, length: 9 cm; reference electrode: silver/silver chloride (Ag/AgCl) diameter: 1 mm, length: 9 cm; counter electrode: 1.5 cm platinum wire fused in glass diameter: 1 mm, length: 9 cm. The electrochemical cell has an inner diameter of 2.5 cm, an outer diameter of 3.2 cm and a height of 4 cm. The scan rate of 100 mV/s was applied with current sensitivity as 0.01 μA.

2.5. Computational details

Quantum mechanical calculations were used to carry out the optimized geometry, NLO, NBO, HOMO–LUMO and TD-DFT with Guassian-03 program using the Becke3–Lee–Yang–Parr (B3LYP) functional supplemented with the standard 6-31G(d,p) basis set [20,21].

2.6. General procedure for the synthesis of Schiff bases (*1*–*6*)

The Schiff bases (**1**–**6**) were synthesized according to the procedure reported in the literature [23]. A solution of *p*-aminoazobenzene (1 mmol) and the corresponding substituted benzaldehydes (1.5 mmol) in 20 ml absolute ethanol was refluxed for 2 h. The resulting precipitate was filtered off and purified by column chromatography.

2.6.1. (0E,4E)-4-(2-phenyldiazenyl)-N-benzylidenebenzenamine (SB*1*)

Yield: 76%, m.p.: 127 °C. Anal. calcd. for $C_{19}H_{15}N_3$: C, 82.41; H, 6.92; N, 10.68. Found: C, 82.02; H, 6.69; N, 10.70. MS: *m*/*z* 262.00, calcd. 262.35. 160.24. ^{1}H NMR: 8.70 (s) CH=N, 6.75 (d) H(2), 7.94 (d) H(3), 7.47 (d) H(5), 6.75 (d) H(6), 8.00 (d) H(42), 7.47(d) H(46), 7.55–7.51 (m) H(44), 7.55–7.51 (m) H(43), 7.55–7.51 (m) H(45), 7.92 (d) H(12), 7.37 (d) H(16), 7.83 (t) H(14), 7.83 (t) H(13), 7.83 (t) H(15). ^{13}C NMR: 161.00 CH=N, 121.53 C(2), 124.01 C(3), 125.02 C(5), 114.53 C(6), 122.24 C(42), 122.71 C(46), 130.76 C(44), 128.94, 128.89, 128.78 C(43), 128.94, 128.89, 128.78 C(45), 129.00 C(12), 129.72 C(16), 131.71 C(14), 128.94, 128.89, 128.78 C(13), 128.94, 128.89, 128.78 C(15), 150.62 C(1), 149.47 C(4), 145.45 C(11), 152.84 C(41).

2.6.2. (0E,4E)-4-(2-phenyldiazenyl)-N-(p-N,N-dimethylaminobenzylidene)benzenamine (SB*2*)

Yield: 76%, m.p.: 127 °C. Anal. calcd. for $C_{21}H_{20}N_4$: C, 76.80; H, 6.14; N, 17.06. Found: C, 76.02; H, 6.02; N, 16.92. MS: *m*/*z* 328.17, calcd. 328.00. ^{1}H NMR: 7.37 (d) CH=N, 8.00 (d) H(2), 7.37 (d) H(3), 6.41 (d) H(5), 8.00 (d) H(6), 8.00 (d) H(42), 7.83 (t) H(44), 7.49–7.39 (m) H(43), 7.49–7.39 (m) H(45), 7.93(d) H(16), 8.27 (d) H(13), 7.49–7.39 (m) H(15), 2.75 (s) CH_3. ^{13}C NMR: CH=N 158.00, 121.23 C(2), 122.76C(3), 124.52 C(5), 115.04 C(6), 122.76 C(42), 124.52 C(46), 131.31 C(44), 129.37 C(43), 129.15 C(45), 122.23 C(12), 130.47 C(16), 132.92 C(14), 130.47 C(13), 127.61 C(15), 154.53 C(1), 151.44 C(4), 153.17 C(41), 40.2 CH_3.

2.6.3. (0E,4E)-4-(2-phenyldiazenyl)-N-(o-methoxybenzylidene)benzenamine (SB*3*)

Yield: 85%, m.p.: 113 °C. Anal. calcd. for $C_{20}H_{17}N_3O$: C, 76.17; H, 5.43; N, 13.32. Found: C, 76.02; H, 6.59; N, 13.12. MS: *m*/*z* 315.37, calcd. 315.02. ^{1}H NMR: 8.45 (s) CH=N, 6.75 (d) H(2), 7.89 (d) H(3), 7.32 (d) H(5), 6.71 (d) H(6), 7.98 (d) H(42), 7.83 (t) H(44), 7.55–7.41 (m) H(43), 7.55–7.41 (m) H(45), 7.92 (d) H(12), 7.55–7.41 (d) H(16), 7.01 (d) H(13), 7.01 (d) H(15), 3.83 (OCH_3). ^{13}C NMR: 160.24 CH=N, 121.53 C(2), 124.00 C(3), 125.02 C(5), 114.53 C(6), 122.24 C(42), 122.67 C(46), 129.72 C(44), 128.89 C(43), 128.89 C(45), 129.10 C(12), 130.72 C(16), 162.46 C(14), 114.53 C(13), 114.19 C(15), 154.70 C(1), 149.47 C(4), 152.84 C(41), 55.39 (OCH_3).

2.6.4. (0E,4E)-4-(2-phenyldiazenyl)-N-(m-hydroxybenzylidene)benzenamine (SB*4*)

Yield: 85%, m.p.: 113 °C. Anal. calcd. for $C_{19}H_{15}N_3O$: C, 75.73; H, 5.02; N, 13.94. Found: C, 75.42; H, 4.69; N, 13.21. MS: *m*/*z* 301.12, calcd. 301.00. ^{1}H NMR: 8.46 (s) CH=N, 7.28 (d) H(2), 7.98 (d) H(3), 7.92 (d) H(5), 7.28 (d) H(6), 7.85–7.76 (m) H(42), 7.85–7.76 (m) H(46), 7.85–7.76 (m) H(44), 7.51–7.31 (m) H(43), 7.51–7.31 (m) H(45), 7.48–7.27 (m) H(16), 6.78–6.73 (m) H(14), 7.48–7.27 (m) H(15), 4.48 (OH). ^{13}C NMR: CH=N 152.87, 122.28 C(2), 122.28 C(3), 124.05 C(5), 121.58 C(6), 122.12 C(42), 125.06 C(46), 129.77 C(44), 129.06 C(43), 128.93 C(45), 114.59 C(12), 129.77 C(16), 128.93

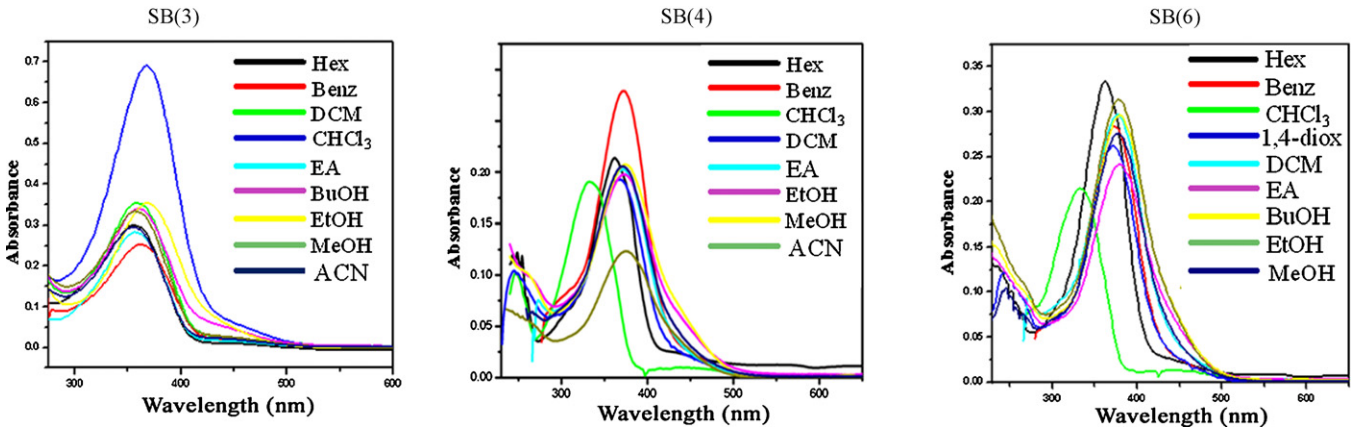

Fig. 1. Absorption spectra of some Schiff bases.

C(14), 125.06 C(13), 125.06 C(15), 122.76 C(1), 122.28 C(4), 129.77 C(11), 125.06 C(41).

*2.6.5. (0E,4E)-4-(2-phenyldiazenyl)-N-(o-hydroxy-m-bromobenzylidene)benzenamine (SB**5**)*

Yield: 75%, m.p.: 156 °C. Anal. calcd. for $C_{19}H_{14}BrN_3O$: C, 60.02; H, 3.71; N, 11.05. Found: C, 59.02; H, 3.29; N, 10.70. MS: *m/z* 379.03, calcd. 379.00. ^{1}H NMR: 8.70 (s) CH=N, 6.75 (d) H(2), 7.94 (d) H(3), 7.47 (d) H(5), 6.75 (d) H(6), 8.00 (d) H(42), 7.55–7.51 (m) H(44), 7.55–7.51 (m) H(43), 7.55–7.51 (m) H(45), 6.95(t) H(16), 7.56–7.54 (m) H(13), 7.05 (t) H(15). ^{13}C NMR: CH=N 163.44, 121.81 C(2), 124.09 C(3), 124.96 C(5), 114.48 C(6), 122.20 C(42), 122.74 C(46), 130.92 C(44), 128.98 C(43), 128.81 C(45), 161.15 C(12), 129.64 C(16), 132.40 C(14), 117.24 C(13), 119.10 C(15), 152.55 C(1), 150.52 C(4), 152.84 C(41).

*2.6.6. (0E,4E)-4-(2-phenyldiazenyl)-N-(p-hydroxy-m-methoxybenzylidene)benzenamine (SB**6**)*

Yield: 80%, m.p.: 118 °C. Anal. calcd. for $C_{20}H_{17}N_3O_2$: C, 72.49; H, 5.17; N, 12.68. Found: C, 72.02; H, 5.69; N, 12.70. MS: *m/z* 331.37, calcd. 331.00. ^{1}H NMR: 8.38 (s) CH=N, 6.72 (d) H(2), 7.29 (d) H(3), 7.85 (d) H(5), 6.72 (d) H(6), 7.98 (d) H(42), 7.85 (t) H(46), 7.85 (t) H(44), 7.49–7.41 (m) H(43), 7.49–7.41 (m) H(45), 7.45 (d) H(12), 7.31(d) H(16), 7.38 (d) H(15), 3.96 (OCH_3), 4.04 (OH). ^{13}C NMR: 160.62 CH=N, 121.58 C(2), 124.07 C(3), 125.07 C(5), 122.13 C(6), 122.29 C(42), 122.72 C(46), 130.76 C(44), 129.06 C(43), 128.85 C(45), 108.50 C(12), 114.58 C(16), 152.68 C(14), 154.60 C(13), 114.24 C(15), 149.32 C(4), 145.46 C(11), 152.87 C(41), 56.04 (OCH_3).

3. Results and discussion

*3.1. Absorption, emission and excitation spectra of Schiff bases (**1**–**6**)*

The UV–visible spectra of the Schiff bases (**1**–**6**) were recorded in protic and aprotic solvents in the region 200–500 nm, the band that appeared around 370.0 nm in dioxane is due to π–π* transition (Fig. 1). Since in aminobenzene dyes, n–π* and π–π* transitions are in close proximity, the low intensity n–π* transition is completely overlaid by the intensive π–π* transition [24]. On comparison with the unsubstituted parent Schiff base (SB**1**), the absorption maximum was blue shifted in the substituted Schiff bases (**2**–**6**) and this may be due to the presence of increased resonance interaction exerted by the substituents. In most of the Schiff bases, the absorption spectra largely depend on the solvent polarity and red shift was observed in hydroxyl solvents. Larger red shift in the absorption band (Table 1) may be due to the stabilizing interaction between the hydroxyl group of the butanol and the substituents of the Schiff bases so that there is greater delocalisation of the π electron cloud of the aromatic system, CH=N and N=N bonds.

The absorption spectrum for the yellowish solution of SB**5** in neutral ethanol show band at 378.1 nm along with a shoulder at 450.2 nm. The addition of different concentrations of NaOH [0–0.017 M] to the ethanol solutions of SB**5** resulted in a single band at 428.0 nm at the expense of both 378.1 and 450.2 nm bands with two isobestic points around 350.0 and 400.0 nm. In cyclohexane, the absorption spectrum of SB**5** shows a single band at 378.1 nm. Therefore, the absorption band at 378.1 nm can be safely assigned to the intramolecularly hydrogen bonded enol form, 428.0 nm is assigned to the anion and 450.2 nm is due to the *cis* enol form of SB**5**, respectively, and the isobestic points confirm the equilibrium among the *trans* enol form, anion and the *cis* enol form (Fig. 2). With increasing base concentration of the solutions of SB**6**, the absorbance at 380.3 nm corresponding to the initially undissociated dye decreases while a new absorbance with a maximum wavelength of 430.0 nm increases and the new absorbance can be attributed to the deprotonated dye. Two isobestic points at 330.0 and 400.0 nm suggest the equilibrium among the *trans* form, anion and *cis* enol form.

All Schiff bases (**1**–**6**) fluoresce strongly in solutions at room temperature (Table 2). The emission spectrum (Fig. 3) for the yellowish solution of SB**5** in neutral ethanol shows a band at 468.0 nm

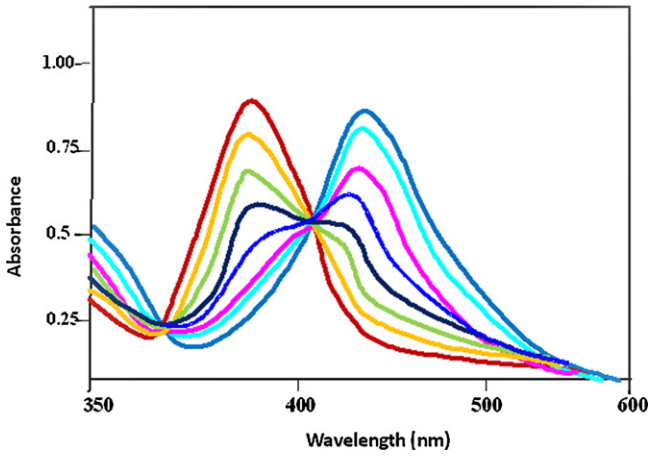

Fig. 2. Absorption spectrum of Schiff base (SB**5**) in ethanol in the presence of sodium hydroxide ([NaOH] = 0–0.017 M).

Table 1
Absorption spectral data (ppm) of Schiff bases **1**–**6**.

Solvents	SB**1** (λ_{max})	SB**2** (λ_{max})	SB**3** (λ_{max})	SB**4** (λ_{max})	SB**5** (λ_{max})	SB**6** (λ_{max})
Cyclohexane	233.5, 364.0	365.4	362.5	362.8	378.1	362.8
Benzene	374.74	333, 368.2	372.3	373.4	361.5	373.8
Chloroform	379.9	333, 367.5	367.5	334.4	376.8	373.3
1,4-Dioxane	382.0	374.0	370.94	372.1	376.0	383.6
Dichloromethane	374.8	368.6	369.5	245, 369.7	361.5	333.8
Ethyl acetate	382.2	370.5	370.4	373.7	369.4	378.2
Acetonitrile	381.6	377.7	371.8	371.7	328, 367.2	377.8
Butanol	384.5	232, 377.7	380/381	372.8	232, 373.5	381.2
Ethanol	383.5	373.7	269/370.8	374.8	378.1, 450.2	380.3

Table 2
Fluorescence spectral data (ppm) of Schiff bases **1**–**6**.

Solvents	SB**1** (λ_{max})	SB**2** (λ_{max})	SB**3** (λ_{max})	SB**4** (λ_{max})	SB**5** (λ_{max})	SB**6** (λ_{max})
Cyclohexane	423.0	418.10	408.5	383.0	525.0 (2699)	412.6
Benzene	441.6	408.50	408.7, 430	383, 400.4	409.5 (3242)	431.1
Chloroform	445.6	427.50	410.0	381.0	423.5 (2921)	383.5
1,4-Dioxane	481.5	421.0	419.2	405.0	450.0, 492.5 (3360)	413.0
Dichloromethane	448.3	420.5	432.2	431.0	433.5 (4594)	426.5
Ethyl acetate	432.0	415.5	417.6	419.5	424.3 (3503)	420.0
Acetonitrile	483.98	448.1	417.6	417.7	413.4 (3043)	419.5
Butanol	491.7	415.6	450.0	427.5	439.2 (4005)	389.0, 408.3
Ethanol	487.1	419.0	410.0	408.0	468.0 (4374)	413.0

Values in the parenthesis are Stoke's shift value.

when excited with 340.0 nm light. The 468.0 nm band is shifted to 508.0 nm when excited with 400.0 nm light. Fig. 4 shows the fluorescence spectra of SB**5** recorded at different pHs and illustrates that the emission is switched 'On' with decreasing pH. It is because at low pH the hydroxyl oxygen is protonated, its oxidation potential raised which switches fluorescence 'On' and at high pH, the intensity of fluorescence emission is low i.e., switched 'Off' due to anion formation which quenches fluorescence.

The excitation spectra of both 468.0 and 508.0 nm emissions of SB**5** show two bands, one band at 358.0 nm and another stronger band at 408.0 nm (Fig. 5). None of the excitation spectrum can explain the absorption spectrum of Schiff base SB**5**. This indicates that the ground and excited state species are different. The excitation spectrum of 495.0 nm in ethanol in the presence of sodium hydroxide occurred at 428.0 nm and are in good agreement with the absorption spectra of SB**5** anion. Therefore, the emission bands at 468.0 and 508.0 nm can be assigned to the intramolecularly hydrogen bonded and *trans* enol and *cis* enol form, respectively, whereas the 428.0 nm band can be assigned to the anion of (SB**5**).

The solid state UV–vis spectra of Schiff bases (**1**–**6**) exhibit absorbances (λ_{max}) at 544.5, 542, 546.3, 566.2, 568.8 and 563.6 nm. The optical band gap value of Schiff bases (**1**–**6**) is found as 2.28, 2.29, 2.27, 2.19, 2.18 and 2.20 eV, respectively, and these are smaller value than the previously reported Schiff base [25]. The smaller band gap indicates easy electronic transitions from bulk to vacuum energy level of the compounds and these compounds have high electrical conductivity as well as fluorescence property. The Stoke's shift values (ΔE) (Table 2) were calculated for SB**5** in all solvents [8] and it is important for a fluorescence sensor. The higher Stoke's shift value supplies very low background signals and resultantly allows the usage of the material in construction of a fluorescence sensor. As seen in Table 2 in comparison with the other solvents, ethanol solution of SB**5** has larger Stoke's shift value than other solvents. This indicates the usage of SB**5** as an ion selective sensor in ethanol solution.

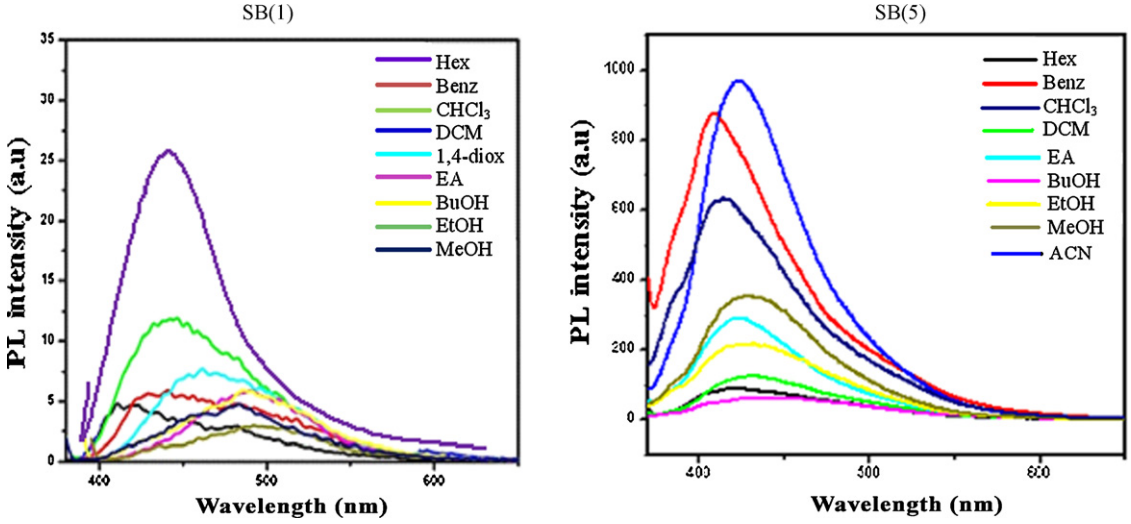

Fig. 3. Emission spectra of some Schiff bases.

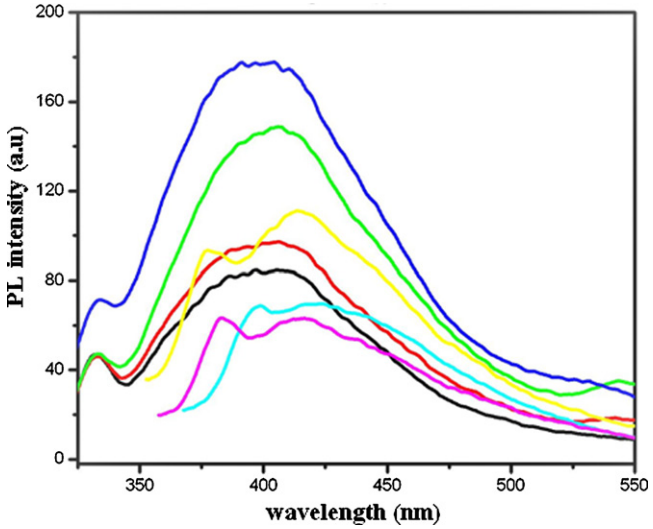

Fig. 4. Emission spectra of Schiff base (SB**5**) by increasing pH.

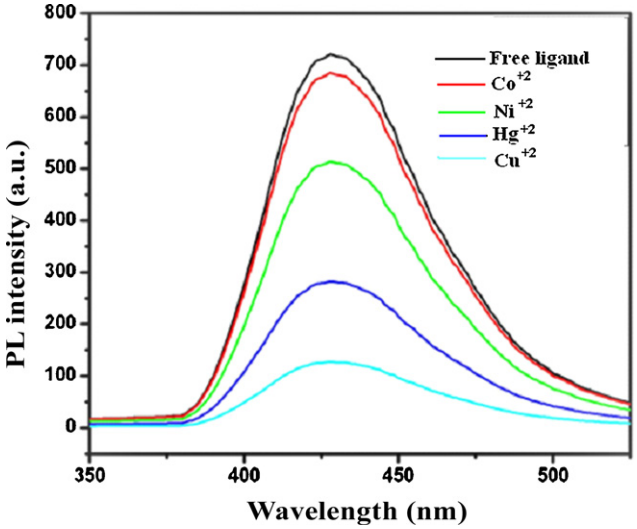

Fig. 6. Fluorescence spectra of Schiff base (SB**5**) in the presence of various metal ions.

3.2. *Schiff base (SB**5**) as a chemosensor*

The changes in the fluorescence properties of SB**5** caused by different metal ions such as Co^{2+}, Hg^{2+}, Ni^{2+} and Cu^{2+} were measured in ethanol. The fluorescence of SB**5** quenched markedly with the gradual addition of Cu^{2+} but the fluorescence properties of SB**5** was influenced by other metal ions (Fig. 6). The fluorescence intensity of SB**5** was linearly reduced with increase in concentration of Cu^{2+} (Fig. 7). According to these spectra when the Cu^{2+} concentrations are 5×10^{-3} and 5×10^{-5} mol/L the relative intensity changes $((I_0 - I)/I_0)$ are 0.80 and 0.27, respectively (Fig. 8). The quenching in fluorescence intensity of Schiff base (SB**5**) by the addition of Cu^{2+} cation indicates the complexation of Schiff base (SB**5**) with Cu^{2+}, the Schiff base (SB**5**) has bidentate sites and forming the expected Cu^{2+} complex (Fig. 9) [25,26]. The possible reason for the fluorescence quenching is the formation of a ground state non-fluorescent complex and the enhancement of spin–orbit coupling [27] for SB**5**–Cu^{2+} is presumed resulting in the fluorescence quenching and the observed linear regression equation is, $((I_0 - I)/I_0) = -0.6680 - 0.3374 \log[Cu^{2+}]$ where, I_0 is the emission intensity of Cu^{2+} free Schiff base (SB**5**), I is the fluorescence intensity of the Schiff base (SB5) in the presence of metal ion Cu^{2+}, and $[Cu^{2+}]$ is the concentration of metal ion. The correlation co-efficient is 0.996. According to the obtained results, Schiff base (SB**5**) can be used as a new fluorescence sensor to detect the quantity of Cu^{2+} ion in any sample solution depending on the relative intensity change.

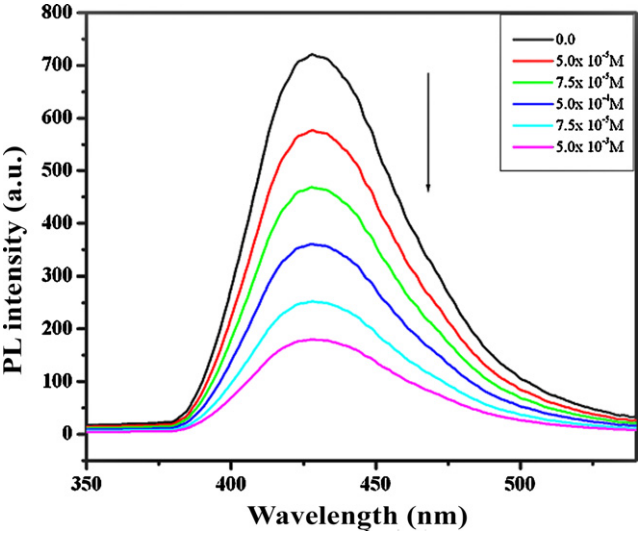

Fig. 7. Fluorescence chemisensors blocking by metal ion binding.

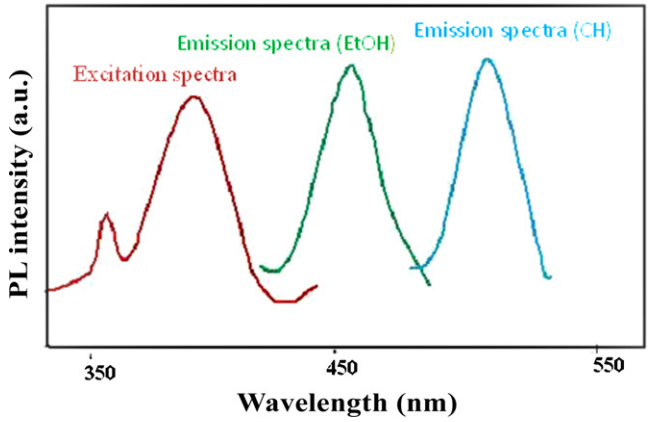

Fig. 5. Excitation and emission spectra of Schiff base (SB**5**).

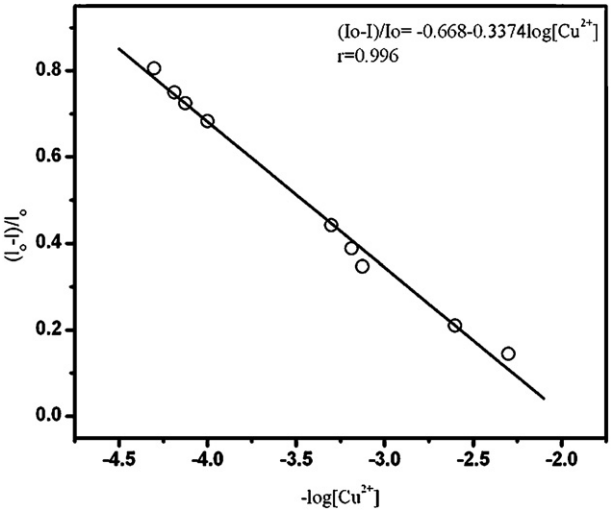

Fig. 8. Plot of normalized intensity $((I_0 - I)/I_0)$ against concentration for Cu^{2+} ion.

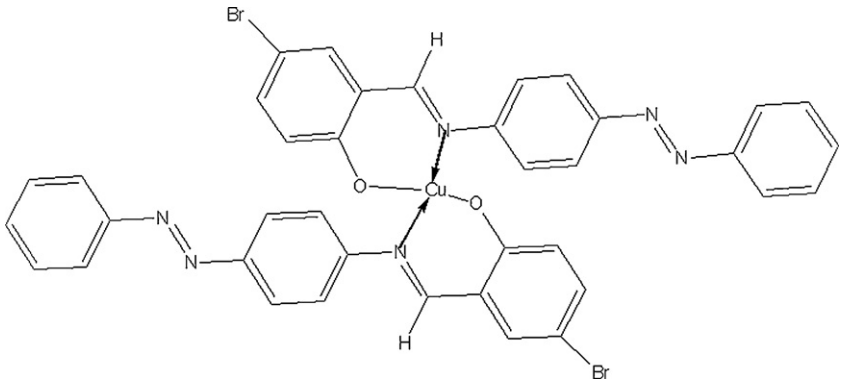

Fig. 9. Possible structure of Schiff base (SB**5**)–Cu^{2+} complex.

The Jobs plot which is extensively used to find the complexation mode in the host–guest interactions [28].

3.3. Photochemical isomerization experiment in solution

The *trans–cis* isomerization of Schiff base SB**2** was carried out and analysed. Fig. 10 shows selected spectra obtained during an experiment of SB**2** in dioxane. At first, the sample was irradiated with light of 374.0 nm which is very close to the maximum absorbance of the π–π* transition. The spectrum obtained after 90 s represents the photo stationary state at this wavelength and the longer irradiation at 374.0 nm did not lead to further changes. Then the excitation wavelength was changed to 420 nm (n–π* transition) to induce the reverse *trans–cis* isomerization and after 60 s a photostationary state was achieved again which differed from that of the non irradiated solution indicating that the latter was already a mixture of both isomers.

3.4. Excited state intramolecular proton transfer (ESIPT) process

It may be suggested that in aprotic solvents, the *o*-hydroxy Schiff base SB**5** exists as intramolecular hydrogen bonded isomers namely *trans* enol I and *cis* enol II (Fig. 11(a)). Excitation of the *trans* enol isomer I should lead to the formation of the keto-isomer III due to ESIPT (Fig. 11(b)). But, we found out that the fluorescence spectra of SB**5** in dioxane contain two emission bands and the emission peak at shorter wavelength at 450.0 nm is assigned to isomer I and the small shoulder peak at higher wavelength 492.5 nm reveal that only the isomer II of SB**5**. However in the case of hydroxyl containing solvent (EtOH), a short wavelength emission band appears for SB**5**. This result corresponds to the data obtained earlier [29–32] for compounds demonstrating ESIPT and can be explained by the presence of intermolecular hydrogen bonding with solvent molecule leading to the stabilization of solvated isomer IV in which ESIPT is impossible.

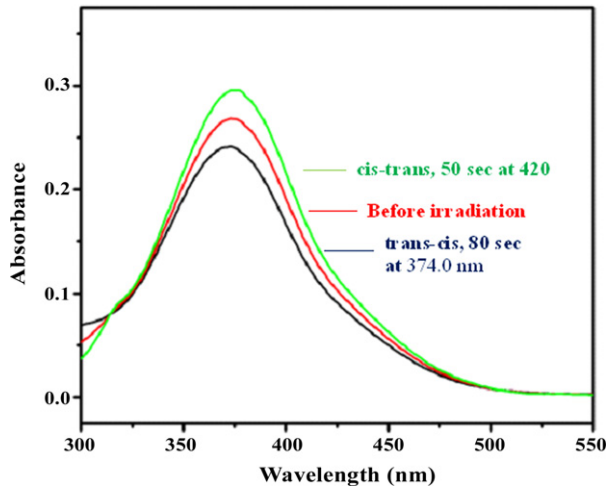

Fig. 10. Photochemical *trans–cis* and *cis–trans* of Schiff base (SB**2**).

For better understanding the ESIPT mechanism in SB**5**, we performed DFT calculation of electron density for the keto and enol isomers of the SB**5** molecule in the ground and the excited states (Table 3) which reveal that excitation of *trans* enol isomer **(I)** leads to an increase in the electron density at N(5) atom and decrease at O atom resulting in ESIPT and formation of the excited keto isomer in excited state. Then, the excited keto isomer emits luminescence and returns to the ground state keto form, which is characterized by a large positive charge at the N(5) atom and negative charge at the O atom. As a result, a reverse process occurs in the ground state of the molecule producing an initial molecule in the enol form.

3.5. Correlation between intramolecular hydrogen bonding and ESIPT process

The existence of intramolecular hydrogen bond in hydroxy substituted Schiff base SB**5** is confirmed by the presence of the singlet at 13.00 ppm in the ^{1}H NMR spectrum (Fig. 12) which is a typical signal for hydrogen bonded hydrogen atom. In order to reveal the contribution of the intramolecular hydrogen bonding in the hydroxy Schiff base SB**5** to their optical properties, the fluorescence spectra of compound SB**5** and its derivative SB**3** were measured in dioxane solvent under identical condition (Fig. 13). A dual fluorescence was detected for SB**5** with emission peak centered at 450.0 and 492.5 nm, respectively. The emission peak at shorter wavelength at 450.0 nm is assigned to isomer I and longer wavelength band at 492.5 nm is assigned to isomer II [31]; whereas compound SB**3** exhibits emission only at 419.2 nm, the absence of additional peak at longer wavelength confirms that the absence of intramolecular hydrogen bond in SB**3** which further evidence that intramolecular hydrogen bond is the essential driving force for ESIPT and the dual fluorescence behaviour of SB**5**.

The competition of intra- and intermolecular hydrogen bonding in Schiff base SB**5** was studied in dioxane–water. A series of

Table 3
Electron density of atoms N(5) and O for Schiff base (SB**5**).

Compound	Atom	I	I*	III
SB**5**	N(5)	−0.456	−0.501	0.423
	O(37)	−0.518	−0.492	−0.586

* Electron density of the atoms in the excited state.

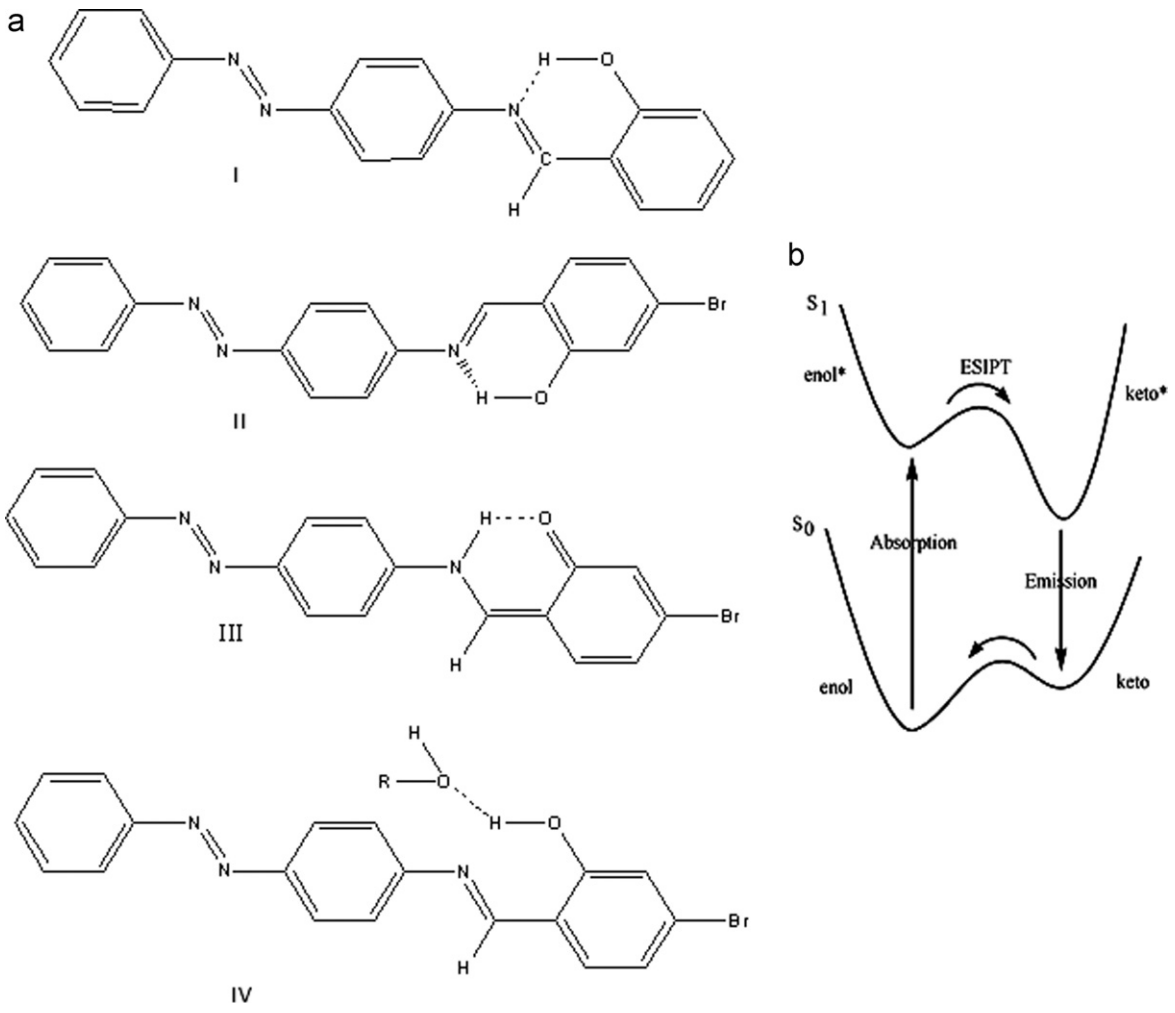

Fig. 11. Various rotameric forms of Schiff base (SB**5**).

solutions in dioxane–water mixture with different water fractions but identical concentrations of SB**5** were made for spectroscopic measurements. Fluorescence spectra of SB**5** exhibit two emission peaks at 450.0 nm (*trans* enol) and 492.5 nm (*cis* enol), respectively, in pure dioxane. With the addition of water, the *trans* enol emission intensity decreases in enol when water fraction is increased to 20% (v/v), the *trans* enol emission almost vanished. With further increasing water fraction to 40% (v/v), a new emission band at 417.0 nm appeared in addition to the normal emission. This band intensity increased with increasing water fraction and turned to be the main emission when water fraction is high up to 80% (v/v). The *trans* enol emission decreases with increasing water fraction in the

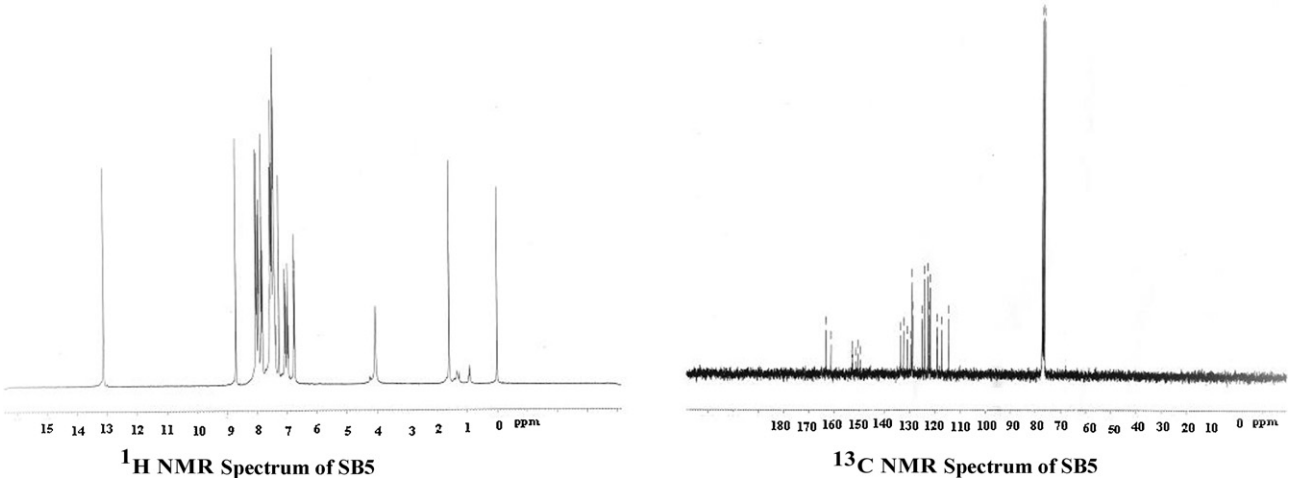

Fig. 12. ^{1}H and ^{13}C spectrum of Schiff base (SB**5**).

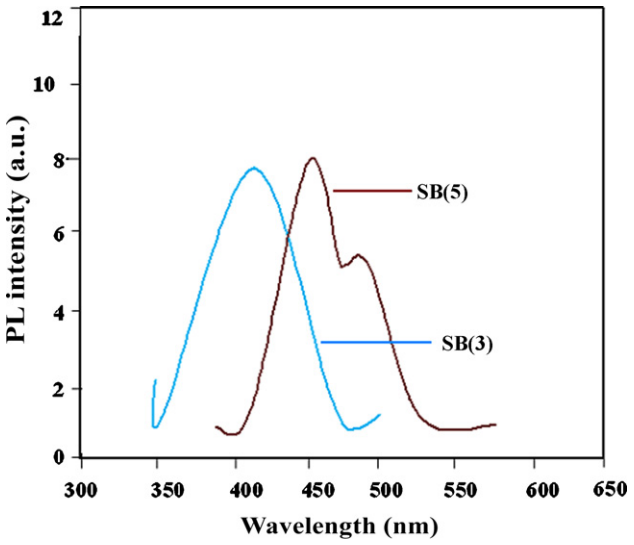

Fig. 13. Fluorescence spectra of Schiff base (SB**5**) and Schiff base (SB**3**).

mixed solvent due to the formation of the intermolecular hydrogen bonding between SB**5** and water. In the initial stage, the presence of small amount of water in the dioxane solution must give rise to the solvation of SB**5**. The intermolecular hydrogen bonding between SB**5** and water definitely disrupts the ground state intramolecular hydrogen bonding isomers but increases the quantity of species IV, in which ESIPT is inhibited and therefore, the *trans* enol emission decreases with addition of water and finally vanished.

3.6. Potential energy surface (PES) studies of Schiff base (SB*5*)

For better understanding the ESIPT mechanism in SB**5**, we performed DFT calculation of electron density for the keto and enol isomers of the SB**5** in the ground and the excited states (Table 3). In the excited state the nitrogen atom becomes richer in electrons than the hydroxylic oxygen atom. This redistribution of the π-electron densities in the excited electronic state is the driving force for the intramolecular proton transfer from the hydroxylic group to the nitrogen atom. Because the ESIPT phenomenon has inspired a large number of theoretical calculations [32–34]. The ground-state geometries of the three species, I–III for SB**5** were optimized using the DFT/6-31G(d,p) method. Complete optimization of all the geometrical parameters gives the ground state energy of each species. The energy of the excited state was calculated using the standard CIS method. Table 4 gives the energies and dipole moment of the species I–III in the ground and the excited states. The potential energy (PE) curves for the interconversion of isomers I and II of SB**5** in the ground (Fig. 14a) and the excited states (Fig. 14b) reveal that for isolated (SB**5**) in the ground state the barrier for interconversion is 4.5 kcal/mol and 3.4 kcal/mol in ethanol. In the excited state the barrier for SB**5** in the isolated molecule and in the ethanol medium is 14.5 and 12.3 kcal/mol, respectively. The barriers for interconversion in the excited state are much higher than that in the ground state (Table 3).

Table 4
Relative energies[a] (kcal/mol) and dipole moments (D) in the ground and excited state for rotamers I, II and III of Schiff base (SB**5**).

Compound	Rotamers	Ground state		Excited state	
		μ (D)	E (kcal/mol)	E (kcal/mol)	μ (D)
SB5	I	4.04	1.05 (0.00)	102.31 (89.95)	8.52
	II	3.26	2.10 (0.79)	108.36 (98.89)	7.89
	III	5.32	15.25 (8.42)	92.58 (345.58)	5.26

[a] Relative energies are calculated with respect to the ground state minimum energy form in ethanol. Values in the parenthesis are recorded in ethanol.

Table 5
Quantum yield and thermodynamic parameters of Schiff bases **1**–**6**.

Compound	ϕ_f	τ_f (ns)	k_r (ns^{-1})	k_{nr} (ns^{-1})	HOMO (a.u.)	LUMO (a.u.)	Eg (a.u.)
SB**1**	0.29	4.8	0.06	0.15	−0.204	−0.088	0.124
SB**2**	0.32	5.1	0.06	0.13	−0.198	−0.084	0.114
SB**3**	0.35	5.5	0.06	0.12	−0.204	−0.084	0.120
SB**4**	0.41	5.6	0.08	0.10	−0.210	−0.090	0.110
SB**5**	0.55	5.9	0.09	0.09	−0.199	−0.087	−0.112
SB**6**	0.52	5.8	0.09	0.08	−0.203	−0.090	0.113

3.7. The decay behaviour of Schiff bases fluorescence

The fluorescence quantum yield for compounds **1**–**6** (Table 5) was measured in acetonitrile using coumarin 47 as a standard. Calculation is done using the following equation

$$\phi_{unk} = \phi_{std}\left(\frac{I_{unk}}{I_{std}}\right)\left(\frac{A_{std}}{A_{unk}}\right)\left(\frac{\eta_{unk}}{\eta_{std}}\right)^2 \quad (1)$$

where ϕ_{unk} is the fluorescence quantum yield of the sample, ϕ_{std} is the fluorescence quantum yield of the standard, and I_{unk} and I_{std} are the integrated emission intensities of the sample and the standard, respectively. A_{unk} and A_{std} are the absorbances of the sample and the standard at the excitation wavelength, respectively. η_{unk} and η_{std} are the indexes of refraction of the sample and standard solutions. The main decay route of the excited state of these compounds (**1**–**6**) and their radiative and non-radiative decay are studied in detail. The radiative (k_r) and non-radiative (k_{nr}) rate constants are calculated by

$$k_r = \frac{\Phi_p}{\tau} \quad (2)$$

$$k_{nr} = \frac{1}{\tau} - \frac{\Phi_p}{\tau} \quad (3)$$

$$\tau = (k_r + k_{nr})^{-1} \quad (4)$$

where $k_r$and k_{nr} are the radiative and non-radiative deactivation, respectively, and τ_f is the life time of the S_1 excited state. The low quantum yields could be explained by non-radiative paths to the low-lying n–π* state of the nitrogen atoms [3].

3.8. HOMO–LUMO energies of Schiff bases (*1*–*6*) by DFT method

The Eigen values of HOMO, LUMO and their energy gap reflect the chemical activity of the molecule and recently the energy gap between the highest occupied molecular orbital (HOMO) and the lowest unoccupied molecular orbital (LUMO) has been used to prove the bioactivity from intramolecular charge transfer (ICT) [35–37]. The HOMO–LUMO energy gap for **1**–**6** was calculated by B3LYP/6-31G(d,p) and from the HOMO–LUMO orbital picture (Fig. 15) of Schiff base (SB**5**), the filled π-orbital (HOMO) is mostly located on the 4-diazenylphenyl ring and centre ring and the unfilled π*-orbital (LUMO) on the 4-diazenylphenyl ring, centre ring and benzylidene ring. On comparison with the parent Schiff base (SB**1**), introduction of electron donating methoxy substituent on the benzylidene ring lowers the energies of both HOMO–LUMO, leading to red shift. The calculation of molecular orbital geometry shows that the visible absorption maxima of the Schiff bases correspond to the electronic transition from HOMO–LUMO. The λ_{max} of the Schiff bases is the function of substituents i.e., the stronger the donar character of the substituent, the more the electrons pushed into the ring and larger λ_{max} [38,39]. The calculated energy

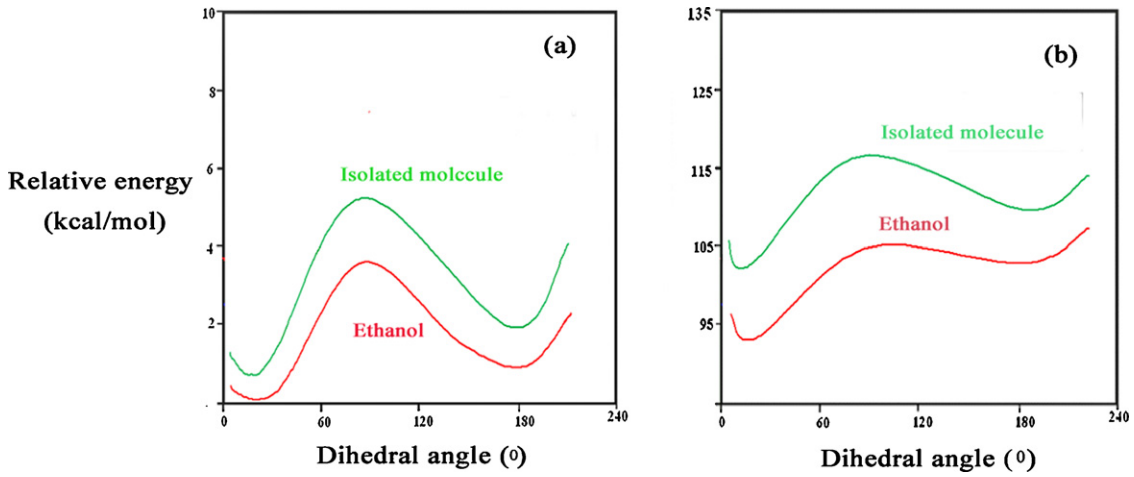

Fig. 14. PES for the interconversion of the rotamers of Schiff base (SB**5**) in the ground state and excited state.

gap explains the eventual charge transfer interactions within the molecule.

3.9. *Relative second harmonic generation (SHG) efficiency of Schiff bases (**1**–**6**)*

Second harmonic signal of 36, 52, 67, 70, 75,and 78 mV was obtained for **1**–**6** by an input energy of 4.1 mJ/pulse. But the standard KDP crystal gave a SHG signal of 110 mV/pulse for the same input energy. The second order nonlinear efficiency will vary with the particle size of the powder sample [40]. Higher efficiencies are achieved by optimizing the phase matching [41]. On a molecular scale, the extent of charge transfer (CT) across the NLO chromophore determines the level of SHG output, the greater the CT and the larger the SHG output.

3.10. *Hyperpolarizability of Schiff bases (**1**–**6**) by DFT method*

In addition to the well known empirical rules to estimate qualitatively the microscopic nonlinear response in Schiff bases (**1**–**6**), DFT calculation is a more accurate prediction of the NLO activity [42,43]. The value of second order optical susceptibility in a given NLO system depends on the molecular hyperpolarizability (β), the number of chromophores and the degree of noncentrosymmetry. From Table 6, it was suggested that these compounds **1**–**6** are polar having non-zero dipole moment, hyperpolarizabilities and hence have well microscopic NLO behaviour [44–46]. To determine the transference region and hence to know the suitability of these compounds **1**–**6** for microscopic nonlinear optical applications, the UV–visible spectra have been recorded using the spectrometer in the range of 190–1100 nm. These compounds show absorption spectra in the UV region. The increased transparency in the visible region might enable the microscopic NLO behaviour with non-zero values [47,48]. All the absorption bands are due to $\pi \rightarrow \pi^*$ transitions. The β values (Table 6) computed here might be correlated with UV–visible spectroscopic data in order to understand the molecular structure and NLO relationship in view of a future optimization of the microscopic NLO properties. Therefore, the validity of B3LYP/6-31G(d,p) approximation used in all the computations here might also be illustrated by analyzing the relationship between calculated β values and measured values of λ_{max} (Table 1). The band at around 370.0 nm exhibits a solvatochromic shift, characteristic of a large dipole moment (Table 6) and frequently suggestive of a large hyperpolarizability (Table 6). These compounds show red shift in absorption with increasing solvent polarity, accompanied with the upward shifts non-zero values in the β-components [20]. From β-values it was found that all these compounds are polar having non-zero dipole moment and such

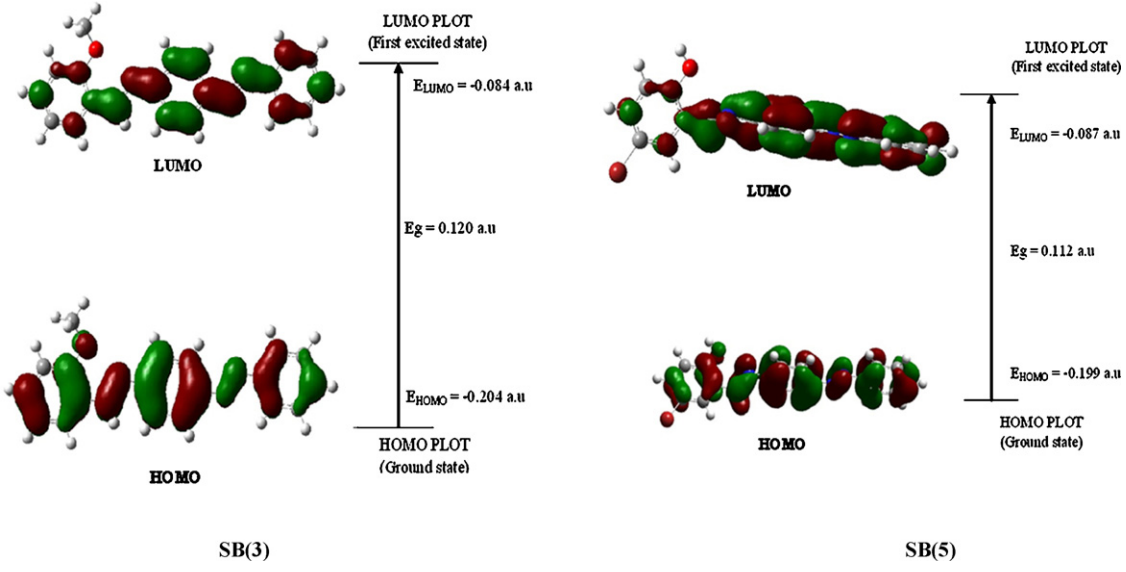

Fig. 15. The atomic orbital compositions of the frontier molecular orbitals of some Schiff bases.

Table 6
Electric dipole moment (D), polarizability (α) and hyperpolarisability (β_{total}) of Schiff bases **1–6**.

Parameter	SB**1**	SB**2**	SB**3**	SB**4**	SB**5**	SB**6**
Electric dipole moment (D)						
μ_x	−0.5062	2.8966	−0.4015	−1.5414	−0.2600	−0.0538
μ_y	−0.0002	−2.5347	−0.8858	4.1739	−0.1390	0.4505
μ_z	0.1859	−1.4794	1.0729	0.8797	1.3629	0.4463
μ_{total}	−0.3203	4.1236	−0.2144	4.5355	0.9639	0.8430
Polarizability (α)						
α_{xx}	223.16	339.8930	180.5289	376.6355	202.2226	−229.4428
α_{xy}	0.0037	−0.1270	34.0782	0.9018	33.8134	37.9341
α_{yy}	69.5529	322.3250	133.8131	338.3096	104.2155	99.4140
α_{xz}	−69.6719	−10.5050	−39.1104	7.0702	−63.2748	−43.7296
α_{yz}	−0.0100	−3.3870	−34.5488	2.9401	−22.5514	−8.5868
α_{zz}	562.5439	166.0810	614.3149	186.6643	604.6976	640.1431
α ($\times 10^{-24}$ esu)	42.2500	40.9180	45.876	44.5400	45.0100	47.8690
Hyperpolarizability (β_{total})						
β_{xxx}	−26.9883	−62.3790	−33.5059	263.5091	−41.3949	−68.8788
β_{xxy}	−0.7929	430.6496	−28.5833	−290.9786	−47.4137	−29.6330
β_{xyy}	−3.1068	115.9535	−14.8611	367.9720	−56.6069	−3.9992
β_{yyy}	1.3538	−176.2216	−93.1900	290.3636	−53.7687	53.4965
β_{yyy}	1.3538	−176.2216	−93.1900	290.3636	−53.7687	53.4965
β_{xxz}	−18.7463	−6.6006	−29.4058	5.1606	9.9654	37.1521
β_{xyz}	−0.9220	17.7301	45.4424	−18.4374	86.6311	60.8972
β_{yyz}	9.1491	13.8175	172.1898	4.2637	110.7366	63.8108
β_{xzz}	379.4481	35.3437	539.3020	−23.3106	324.3709	478.3876
β_{yzz}	0.2850	−37.7675	202.4031	34.0360	−170.6665	21.3076
β_{zzz}	−3268.37	−9.7975	−7631.11	6.6751	−3806.45	−8608.00
β ($\times 10^{-31}$ esu)	28.479	20.2340	64.8360	52.6420	31.9890	73.5900

compounds have large hyperpolarizabilities and hence have rather well microscopic NLO behaviour [49].

3.11. Redox properties

The redox behaviour was examined by cyclic voltammetric technique. When compared with parent compound ($E_{1/2}$ = −1.10 V), the observed negative $E_{1/2}$ values (−1.43 to −1.56) show that the increased ease of reduction of Schiff bases as a consequence of its better is π-accepting characteristics as the result of an increased in its extended π-conjugation [50].

3.12. Conformation of Schiff bases (*1–6*)

Comparison of the chemical shifts of azomethine proton in the Schiff bases (**1–6**) with that of aldehydic proton in their corresponding substituted benzaldehydes reveals that considerable shielding has been observed due to the conversion of parent aldehydes to Schiff bases. Generally in Schiff bases, the bulky group adopts *trans* orientation. Therefore, it is inferred that the azomethine proton is *syn* to diazenophenyl benzenamine ring in Schiff bases (**1–6**). Therefore, the favoured conformation of the Schiff bases (**1–6**) is predicted to be the *anti* conformation i.e., the CH=N and N=N groups are anti to each other.

Generally for the Schiff base derived from *p*-aminoazo benzene, there are two possible conformations (**A** and **B**) with respect to the CH=N and N=N groups shown. In the planar *anti* conformation **A**, the CH=N and N=N bonds are *trans* to each other whereas in the planar *syn* conformation **B**, the CH=N bond and N=N bond are *cis* to each other. Therefore, these two conformations are labelled as *anti* (**A)** and *syn* (**B)** conformations, respectively. To predict the favoured conformation DFT calculation was made using B3LYP/6-31G(d,p) basis set for the Schiff bases (**1–6**). From the heat of formation values it is predicted that all Schiff bases exist as an equilibrium mixture of the conformer *anti* (**A**) (major) with little contribution of *syn* **B** conformer.

4. Conclusion

Intermolecular hydrogen bonding of Schiff base (SB**5**) with water giving rise to IV impedes the ESIPT process. However, the intermolecular hydrogen bonding with alcohol is not strong enough to compete with the intramolecular hydrogen bonding in hydroxy substituted Schiff base. With increasing base concentration of the solutions of hydroxy substituted Schiff bases (SB**4** and SB**5**), two isobestic points are found which confirm the equilibrium among the *trans* enol form, anion and the *cis* enol form. The fluorescence of SB**5** quenched markedly with the gradual addition of Cu^{2+} but the fluorescence properties of SB**5** was influenced by other metal ions. Therefore Schiff base (SB**5**) can be used as a new fluorescence sensor to detect the quantity of Cu^{2+} ion in any sample solution depending on the relative intensity change. The DFT calculations indicate that excitation of rotamer II molecule leads to increase in the electron density at the N(5) atom and decrease at O atom resulting in ESIPT and formation of the excited keto isomer III in excited state. Then, the excited keto isomer III emits luminescence and returns to the ground state keto form III, which is characterized by large positive charge at the N(5) atom and negative charge at the O atom. As a result, a reverse process occurs in the ground state of the molecule, producing an initial molecule in the form enol. In the excited state, the nitrogen atom becomes richer in electrons than the hydroxylic oxygen atom. This redistribution of the π-electron densities in the excited electronic state is the driving force for the intramolecular proton transfer from the hydroxylic group to the nitrogen atom. PES calculation reveals that the barriers for interconversion in the excited state are much higher than that in the ground state. Our further work to focuson the increased transparency of Schiff base derivatives in the visible region might enable the microscopic NLO behaviour with non-zero values and all the absorption bands are due to only π–π^* transition. The higher value of specific heat shows that these compounds are more resistant to laser damage threshold compared to potassium dihydrogen phosphate. Its phase matching and relative second harmonic generation efficiency was determined using Nd:YAG laser as a source. Its electric dipole moments, polarizability, hyperpolarisability and HOMO–LUMO energies studies were determined by DFT calculation.

Acknowledgments

One of the author Dr. J. Jayabharathi, Associate Professor in Chemistry, Annamalai University is thankful to Department of Sci-

ence and Technology [No. SR/S1/IC-07/2007] and University Grants Commission (F. No. 36-21/2008 (SR)) for providing fund to this research work.

References

[1] K. Nejati, Z. Rezvani, B. Massoumi, Dyes Pigm. 75 (2007) 653.
[2] E. Peker, S. Serin, Synth. React. Inorg. Met.-Org. Chem. 34 (2004) 859.
[3] P. Souza, J.A. Garcia-Vazquez, J.R. Masaguer, Transition Met. Chem. 10 (1985) 410.
[4] H. Naeimi, J. Safari, A. Heidarnezhad, Dyes Pigm. 73 (2007) 251.
[5] S.J. Lippard, J.M. Berg, Principles of Bioinorganic Chemistry, University Science Books, California, 1994.
[6] Y.W. Wang, Y.T. Shi, Y. Peng, A.J. Zhang, T.H. Ma, W. Dou, J.R. Zheng, Spectrochim. Acta A 72 (2009) 322.
[7] N. Shing, N. Kaur, J. Dunn, M. MacKay, J.F. Callan, Tetrahedron Lett. 50 (2009) 953.
[8] O. Oter, K. Ertekin, R. Kilincarslan, M. Ulusoy, B. Cetinkaya, Dyes Pigm. 74 (2007) 730.
[9] L. Guo, S. Hong, X. Lin, Z. Xie, G. Chen, Sens. Actuators B 130 (2008).
[10] G. Farrugia, S. Lotti, L. Prodi, N. Zaccheroni, M. Montalti, P.B. Savage, G. Andreani, V. Trapani, F.I. Wolf, J. Fluoresc. 19 (2009) 11.
[11] N. Aksuner, E. Henden, I. Yilmaz, A. Cukurovali, Sens. Actuators B 134 (2008) 510.
[12] G.K. Li, Z.X. Xu, C.F. Chen, Z.T. Huang, Chem. Commun. 15 (2008) 1774.
[13] V. Dujols, F. Ford, A.W. Czarnik, J. Am. Chem. Soc. 119 (1997) 7386.
[14] H.J. Kim, S.Y. Park, S. Yoon, J.S. Kim, Tedrahedron 64 (2008) 1230.
[15] H.L. Mu, R. Gong, Q. Ma, Y.M. Sun, E.Q. Fu, Tedrahedron Lett. 48 (2007) 5525.
[16] J. Xie, M. Menand, S. Maisonneuve, R. Metivier, J. Org. Chem. 72 (2007) 5980.
[17] Y.J. Mei, P.A. Bentley, W. Wang, Tedrahedron Lett. 47 (2006) 2447.
[18] M. Kurtog'lu, E. Ispir, M. Kurtog'lu, S. Serin, Dyes Pigm. 77 (2008) 75.
[19] E. Ispir, Dyes Pigm. 82 (2009) 13.
[20] Guassian 03 Program, Gaussian Inc., Wallingford, CT, 2004.
[21] H.B. Schlegel, J. Comput. Chem. 3 (1982) 214.
[22] S.K. Kurtz, T.T. Perry, J. Appl. Phys. 39 (1968) 3798.
[23] S.P. Scott, Radom, J. Chem. Phys. 100 (1996) 16562.
[24] G. Gabor, Y.F. Frei, E. Fischer, J. Phys. Chem. 72 (1968) 3266.
[25] M. Yildirim, I. Kaya, J. Fluoresc. 20 (2010) 771.
[26] M. Yildirim, I. Kaya, J. Inorg. Organomet. Polym. 18 (2008) 325.
[27] D.S. McClure, J. Chem. Phys. 20 (1952) 682.
[28] H.J. Schneider, A. Yatsimirsky, Principles and Methods in Supramolecular Chemistry, John Wiley & Sons, Chichester, 2000, p. 151.
[29] H.A. Benesi, J.H. Hildebrand, J. Am. Chem. Soc. 71 (1949) 2703.
[30] M. Barra, C. Bohne, J.C. Scaiano, J. Am. Chem. Soc. 112 (1990) 8075.
[31] K. Das, N. Sarkar, A.K. Ghosh, D. Majumdar, D.N. Nath, K. Bhattacharyya, J. Phys. Chem. 98 (1994) 9126.
[32] P.F. Barbara, P.K. Walsh, L.E. Brus, J. Phys. Chem. 93 (1989) 29.
[33] G.J. Woolfe, M. Melzig, S. Schneider, F. Dorr, Chem. Phys. 77 (1983) 213.
[34] A.L. Sobolewski, Chem. Phys. Lett. 211 (1993) 293.
[35] K. Fukui, T. Yonezawa, H. Shingu, J. Chem. Phys. 20 (1952) 722.
[36] L. Padmaja, C. Ravikumar, D. Sajan, I. Hubert Joe, V.S. Jayakumar, G.R. Pettit, O. Faurskov Neilsen, J. Raman Spectrosc. 40 (2009) 419.
[37] C. Ravikumar, I. Hubert Joe, V.S. Jayakumar, Chem. Phys. Lett. 460 (2008) 552.
[38] Q. Sun, Z. Li, X. Zeng, M. Ge, D. Wang, J. Mol. Struct. (Theochem) 724 (2005) 167.
[39] S.Y. Chai, R. Zhou, Z.W. An, A. Kimura, K. Fukuho, M. Matsumura, Thin Solid Films 479 (2005) 282.
[40] Y. Porter, K.M. OK, N.S.P. Bhuvanesh, P.S. Halasyamani, Chem. Mater. 13 (2001) 1910.
[41] M. Narayana Bhat, S.M. Dharmaprakash, J. Cryst. Growth 236 (2002) 376.
[42] A. Karakas, A. Elmali, H. Unver, I. Svoboda, J. Mol. Struct. 702 (2004) 103.
[43] H. Unver, A. Karakas, A. Elmali, J. Mol. Struct. 702 (2004) 49.
[44] I.S. Lee, D.M. Shin, Y. Yoon, S.M. Shin, Y.K. Chung, Inorg. Chim. Acta 343 (2003) 41.
[45] C. Mang, K. Wu, M. Zhang, T. Hong, Y. Wei, J. Mol. Struct. (Theochem) 674 (2004) 77.
[46] K.R. Justin Thomas, J.T. Lin, Y.S. Wen, J. Organomet. Chem. 575 (1999) 301.
[47] S.G. Prabhu, P.M. Rao, S.I. Bhat, V. Upadyaya, S.R. Inamdar, J. Cryst. Growth 233 (2001) 375.
[48] V. Crasta, V. Ravindrachary, R.F. Bharantri, R. Gonsalves, J. Crystal Growth 267 (2004) 129.
[49] F. Volmer, W. Rettig, J. Photochem. Photobiol. A: Chem. 95 (1996) 143.
[50] H.C. Wu, P. Thanasekaran, C.H. Tsai, J.Y. Wu, S.M. Huang, Y.S. Wen, K.L. Lu, Inorg. Chem. 45 (2006) 295.